## Supplementary Materials

### *Preconditioning in preterm mice*

Swiss mice were injected *i.p.* with a single dose of $MgSO_4$ (0.92 mg/g n=7) (Magnesiumsulphate, 1 mmol/ml, Addex; Fresenius Kabi, Halden, Norway) or an equivalent volume of vehicle (n=4) (Saline 9 mg/ml, B Braun Melsungen AG, Melsungen, Germany) 24 h prior to ibotenate. Pups were then returned to their dams.

### *Excitotoxic model of brain injury in preterm mice*

10 µg ibotenate (Sigma, Saint Louis, MO, U.S.A.) diluted in PBS containing 0.02 per cent acetic acid was administered via intracerebral injection as previously described (1). Injections were on anesthetized pups (isoflurane 2 per cent, Zoetis, Paris, France) with a 26G needle on a 50 µl Hamilton syringe mounted on a calibrated microdispenser (PB600-1, Hamilton, Reno, Nevada, USA). The needle was inserted 2 mm under the external surface of scalp skin in the frontoparietal area of the right hemisphere, 2 mm from the midline in the lateral-medial plane and 3 mm from the junction between the sagittal and lambdoid sutures in the rostro-caudal plane. Two 1 µl boluses were injected at a 30-second interval. In all cases, the tip of the needle reached the periventricular white matter. After the injections, pups were returned to their dams.

### *Lesion size determination*

Five days after intracerebral ibotenate injection (PND10), pups were sacrificed and brains immersion fixed in formaldehyde (VWR Q-Path Chemicals, Radnor, PA, USA) for five days. Brains were paraffin embedded and serially sectioned in a microtome (MM, Microm, Brignais, France) into 15 µm coronal sections from frontal to occipital poles. Every third section was stained with cresyl-violet (Merck, Darmstadt, Germany), permitting for accurate and reproducible microscopical determination (Nikon Eclipse E200) of the maximal sagittal fronto-occipital diameter, which is a function of the number of sections containing the lesion and the width of each section. The maximal diameter was defined as the length of the lesion in the sagittal fronto-parietal axis (2). This measure was also used as an index of lesion volume (Supplementary Fig. 1).

*$MgSO_4$ affects the metabolome in the brain*

Rat pups were injected with $MgSO_4$ or vehicle and exposed to 60 minutes HI 24 h later or left as untreated. Samples of cerebral cortex were prepared at 3 or 24 h post injection or directly following 60 minutes HI and analyzed with proton nuclear magnetic resonance ($H^+$-NMR) using Mplot, detecting 119 features. Orthogonal projections to latent structures – discriminant analysis (OPLS-DA) was used to find separations pairwise within the groups and in order to check whether the three groups (3 h, 24 h and 60 minutes HI) could be separated from each other, a Partial least squares – discriminant analysis (PLS-DA) was performed (Supplementary Fig. 2).

*O2k-Fluorometry*

Mitochondrial reactive oxygen species (ROS) formation can be detected with an $H_2O_2$ sensitive probe since the primary chemical ROS-produced species (the superoxide anion) is immediately converted to $H_2O_2$ by mitochondrial superoxide dismutase (MnSOD).The most pronounced $H_2O_2$ flux changes were observed for succinate and rotenone (3). A CII-linked protocol measuring respiration and $H_2O_2$ flux simultaneously in the O2k-Fluorometer was applied. The $H_2O_2$-sensitive probe Amplex® UltraRed (10 µM), horseradish peroxidase (1 U/mL) and SOD (2 µl, f.c. 5 U/ml)) was added to the chamber. The Amplex Red and $H_2O_2$ reaction product is catalyzed by horseradish peroxidase producing fluorescence. Calibrations were performed with $H_2O_2$ (0.1 µM). For ROS production measurements, mitochondria were stimulated with ADP followed by rotenone, blocking Complex-I mediated respiration, allowing for the study of ROS produced solely at Complex-II driven by succinate addition. To induce maximal respiration/ROS production, FCCP (1 µM) was added. Volume-specific $H_2O_2$ fluxes were calculated real-time (DatLab software, OROBOROS INSTRUMENTS, Innsbruck Austria). The stable portions of the $H_2O_2$ fluxes were selected and artifacts induced by addition of substrates/chemicals were excluded. Values were normalized to total protein content (4-6).

*Metabolomics*

Cortex homogenates were lyophilized overnight and re-dissolved in 220 µl buffer (37.5 mM sodium phosphate pH 6.95, 100 per cent $D_2O$, 0.02 per cent $NaN_3$, 0.25 mM DSS-d6, 1 mM

imidazole added directly before use from a 1M stock in $H_2O$). Samples were shaken at 800 rpm for 5 min (12°C) (Eppendorf Thermomixer Comfort) and spun down for 1 min at 1000 g (4°C) (Eppendorf 5804 R centrifuge, FA-45-30-11 rotor). Supernatants (200 µl) were transferred to 3 mm Sample Jet tubes using a Bruker SamplePro L liquid handling robot (Bruker Biospin, Rheinstetten, Germany). Serum samples (100 µl) were mixed with 100 µl buffer (75 mM sodium phosphate pH 7.4, 20 per cent $D_2O$, 2 mM imidazole, 0.04 per cent $NaN_3$, 0.5 mM DSS-d6) in a deepwell plate (Sarstedt, Megablok 1.2 ml) and transferred to 3 mm SampleJet tubes (Bruker Biospin) with a Bruker SamplePro L liquid handling robot. All racks/sample tubes were kept in cooling positions on the robot during transfer. NMR data for serum and cortex samples were acquired on an Oxford 800 MHz magnet equipped with a Bruker Avance III HD console and a 3 mm TCI cryoprobe (Bruker BioSpin, Rheinstetten, Germany). A cooled SampleJet automatic sample changer (Bruker BioSpin) kept the temperature of the samples in the experimental acquisition queue (6 °C). Sample data was acquired with a 1D Carr–Purcell–Meiboom–Gill (CPMG) perfect-echo experiment with excitation sculpting for water suppression. The CPMG pulse train duration was 193 ms with a sweep width of 20 ppm and 128 (serum) or 256 (cortex) scans/experiment,a relaxation delay of 1.3 s and a data acquisition period of 2.04 s. Data was acquired into 65536 complex points. Temperature during data acquisition was 25°C. All spectra were processed in TopSpin 3.5 pl1 (Bruker GmbH, Rheinstetten, Germany). The spectra were zero filled to 131072 real points and fourier transformed within Topspin 3.5 pl1 (Bruker GmbH, Rheinstetten, Germany). Thereafter they were loaded and processed within MATLAB (Release 2015a, The MathWorks, Inc., Natick, Massachusetts, United States.) using in house scripts aiding manual peak/feature identification, (where a feature could be e.g. a doublet obviously belonging to the same molecule type) prior alignment using icoshift (7, 8) and subsequent summation of the peak or feature to the baseline. The peak or feature intensities for each spectrum were normalized using probabilistic quotient normalization (9) to median data sets of the serum and cortex intensities respectively. In addition to the original ipsi- and contralateral cortex feature intensity lists, two additional lists with the sum and difference between the ipsi- and contralateral cortex values for each animal were also created. 403 peaks (features) were identified in serum and 119 in cortex. For serum, 310 features could be annotated to 131 different molecules or combinations of overlapping molecules or lipids. 44 different molecules were annotated to at least one unique feature. For cortex the same numbers were 88, 43 and 31. Multivariate analysis of the serum and cortex features and intensity lists were made using standard procedures in Simca (Version 14.1.0.2047, Umetrics AB). Since the

intensity lists were constructed with care also for smaller sized peaks these were examined mainly using UV- scalingand then Pareto- scaling was used as an imprecise extra validation making sure that different scaling would not give conflicting results. PCA was used to find outliers and get an overview of the data set. All serum- and cortex- intensity lists were kept, one variable was excluded since it only had intensity in a few samples and seemed unlikely to give meaning in the study. PLS-DA, OPLS-DA and OPLS-EP (10) models were constructed to find molecule concentrations discriminating between treatment with $MgSO_4$ or vehicle, the different times treatment had been given and the ipsi- or contralateral hemispheres.

## Supplementary Figures

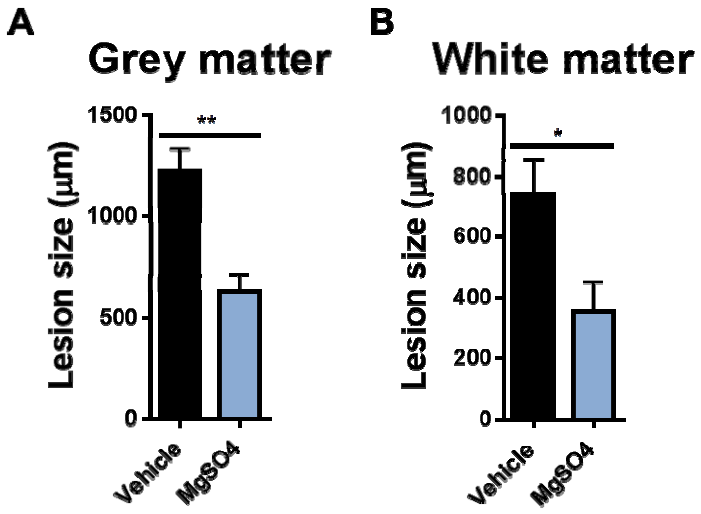


*Supplementary Fig. 1* ***Evaluation of brain injury following $MgSO_4$ pre-treatment in the excitotoxic model of brain injury in preterm mice.***

Assessment of brain injury in a PND 5 mouse model of excitotoxicity (ibotenate; 10 µg) demonstrating attenuation of the **(A)** grey ($p<0.01$) and **(B)** white ($p<0.05$) matter (cresyl-violet) lesion size after injection with $MgSO_4$ (0.92 mg/g) 24 h before ibotenate injection compared to vehicle (Mann Whitney U test, Mean $\pm$ SEM).

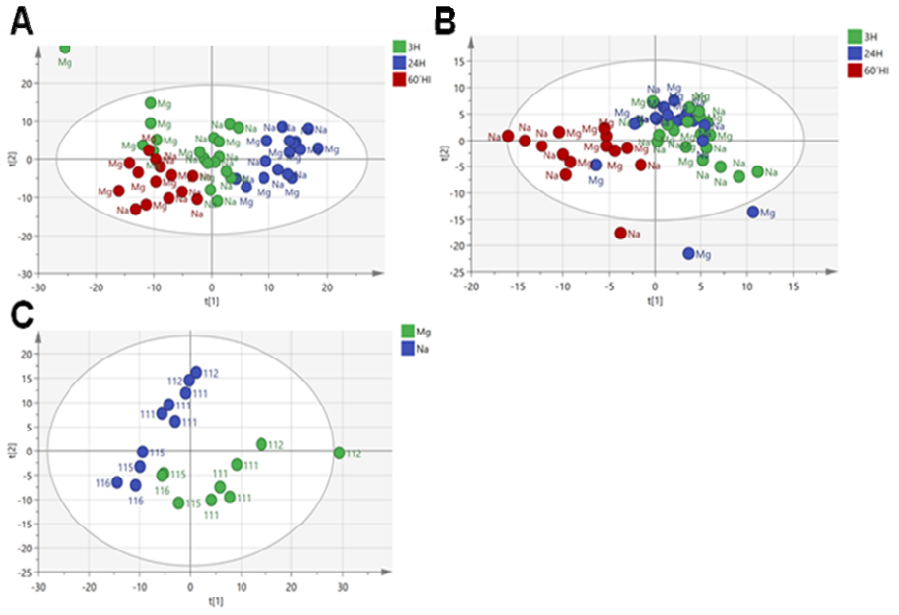


*Supplementary Fig. 2.* ***Principal Component Analysis (PCA) data.***

**(A)** PCA of serum samples. Differences in the samples allows for clear separation of the groups (3 h (green), 24 h (blue) and 60 min HI (red)). **(B)** PCA of samples from cerebral cortex. 60 min HI samples are clearly separated from the two control groups (3 h and 24 h). **(C)** PCA of serum samples collected 3 h post $MgSO_4$/NaCl injection showing separation between $MgSO_4$ and vehicle groups.

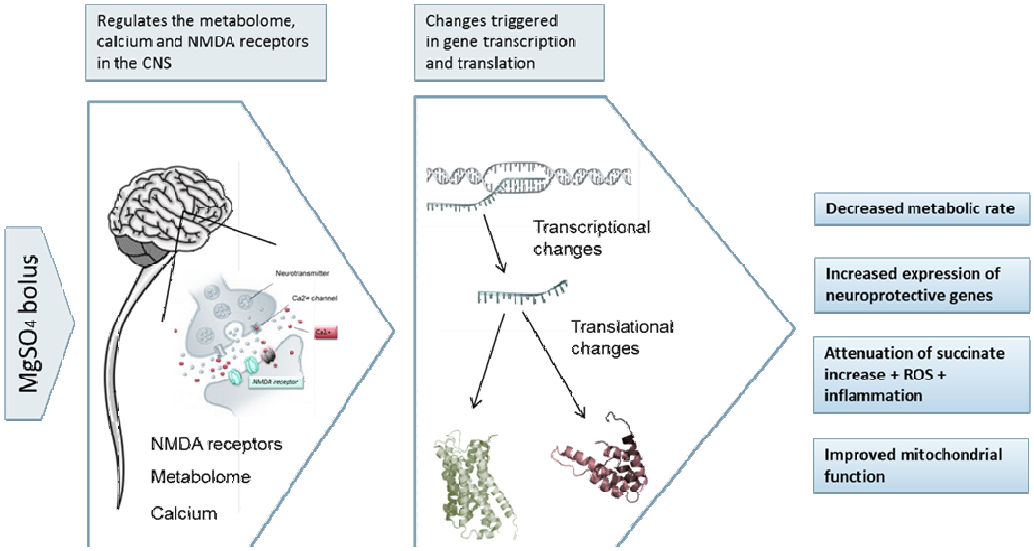


*Supplementary Fig 3.* ***Hypothetical scheme.***

Tentative mechanisms behind $MgSO_4$ preconditioning of the immature brain.

## Supplementary Tables

| Score | Criteria |
|---|---|
| **0** | Normal |
| **0.5** | Almost completely normal<br>Left hemisphere slightly smaller |
| **1** | Plaque on surface, minimal hypotrophy |
| **1.5** | Gradually more pronounced hypotrophy, with or without plaque |
| **2** | Obvious cavitations/loss of tissue |
| **2.5** | Cysts are added |
| **3** | Only midline left |
| **3.5** | Only frontal cortex left |
| **4** | No left hemisphere |

*Supplementary Table 1.* ***Brain injury scoring system of gross morphology.***

| | |
|---|---|
| Rn_Hk2 | QT00190764 |
| Rn_Mt2A | QT01813112 |
| Rn_Fkbp5 | QT01617847 |
| Rn_Hif3α | QT00189854 |
| Rn_Ywhaz | QT02382184 |

*Supplementary Table 2.* ***Primers used for RT-PCR.***

| Gene | Gene ID | Ensemble # | Fold change | P-value | Time point | Ref |
|---|---|---|---|---|---|---|
| Metallothionein 2A | Mt2A | ENSRNOT00000067 | +1.36 | 0.028 | 3h | (11) |
| Oncostatin M receptor | Osmr | ENSRNOT00000040 | +1.41 | 0.038 | 3h | (12) |
| Erythropoietin | Epo | ENSRNOG00000001412 | +1.18 | 0.024 | 3h | (13) |
| Hypoxia inducible factor 3 alpha subunit | HIF3a | ENSRNOG00000017198 | +1.34 | 0.0017 | 3h | (13-15) |
| Hypoxia-inducible factor 1, alpha subunit inhibitor | Hif1an | ENSRNOG00000014234 | +1.11 | 0.005 | 24h | (13-15) |
| Hypoxia inducible factor 1, alpha subunit | Hif1a | ENSRNOG00000008292 | -1.04 | 0.040 | 24h | (13-15) |
| Sirtuin 4 | Sirt4 | ENSRNOG00000001151 | +1.10 | 0.013 | 3h | (16) |
| Heat shock protein 5 | Hspa5 | ENSRNOG00000018294 | -1.13 | 0.0031 | 3h | (17) |
| Heat shock protein 90, beta, member1 | Grp94 | ENSRNOG00000026963 | -1.09 | 0.028 | 3h | (18, 19) |
| Heat Shock protein 1 | Hsp60 | ENSRNOT00000019 | -1.07 | 0.017 | 3h | (20, 21) |
| Heat Shock protein 14 (HSP70 family) | Hspa14 | ENSRNOG00000015212 | +1.06 | 0.023 | 24h | (21, 22) |
| Protein kinase, AMP-activated, gamma 3 non-catalytic subunit | Prkag3 | ENSRNOG00000017248 | +1.18 | 0.048 | 3h | (23, 24) |
| Protein kinase, AMP-activated, beta 1 non-catalytic subunit | Prkab1 | ENSRNOG00000001142 | -1.09 | 0.04 | 24h | (23, 24) |
| Protein kinase, AMP-activated, beta 2 non-catalytic subunit | Prkab2 | ENSRNOG00000018166 | +1.09 | 0.015 | 3h | (23, 24) |
| Hexokinase 2 | HK2 | ENSRNOG00000006116 | -1.10 | 0.0080 | 3h | (25) |

*Supplementary Table 3.* ***Genes regulated after $MgSO_4$ implicated in tissue vulnerability or preconditioning.***

| Micro RNA | family | Ensemble # or MiRNA base | Fold change | P-value | Tentative Targets/regulators | Time point | Ref |
|---|---|---|---|---|---|---|---|
| Mir-143-5p | Mir143 | ENSRNOG00000035603 | -1.33 | 0.010 | Prkce | 3h | (26) |
| Mir-297a-3p | Mir297 | ENSRNOG00000036251 | +1.74 | 0.038 | Creb1,hox1 | 3h | (27) |
| Mir-466 | Mir466 | ENSG00000265376 | +1.22 | 0.040 | IGF1, Smad 2/3 | 3h | (28) |
| Mir-467 | Mir467 | ENSMUSG00000096624 | +1.22 | 0.030 | IGF1, Smad 2/3 | 3h | (28) |
| Mir-467 | Mir467 | ENSMUSG00000096624 | +1.58 | 0.048 | IGF1, Smad 2/3 | 24h | (28) |
| Mir-1-3p | Mir1 | miRBase:MI0003489 | -1.19 | 0.039 | BDNF, KCJN2 | 3h | (29-32) |
| Mir-1-3p | Mir1 | miRBase:MI0003489 | -1.88 | 0.010 | BDNF, KCJN2 | 24h | (29-32) |
| Mir-101-5p | Mir101 | ENSRNOG00000035532 | +1.21 | 0.010 | Pi3K,Akt,TGFb | 3h | (33) |
| Mir-101-3p | Mir101 | ENSRNOG00000035532 | -1.51 | 0.021 | Pi3K,Akt,TGFb | 24h | (33) |
| Let-7 | MIRLET7 | miRBase:MI0004968 | -1.16 | 0.023 | MYC, BCL2L1 | 3h | (28, 34) |
| Mir-199a-5 | Mir199 | miRBase:MI0006890 | +1.57 | 0.045 | Hif1a, sirt1 | 24h | (35-37) |
| Mir-23a | Mir23 | ENSRNOG00000035644 | -1.13 | 0.027 | MYC, tgfb1 | 24h | (38) |

*Supplementary Table 4.* ***miRs regulated after $MgSO_4$ implicated in preconditioning or tissue vulnerability.***

## References


1. Dommergues MA, Patkai J, Renauld JC, Evrard P, Gressens P. Proinflammatory cytokines and interleukin-9 exacerbate excitotoxic lesions of the newborn murine neopallium. Ann Neurol. 2000;47(1):54-63.
2. Medja F, Lelievre V, Fontaine RH, Lebas F, Leroux P, Ouimet T, et al. Thiorphan, a neutral endopeptidase inhibitor used for diarrhoea, is neuroprotective in newborn mice. Brain. 2006;129(Pt 12):3209-23.
3. Makrecka-Kuka M, Krumschnabel G, Gnaiger E. High-Resolution Respirometry for Simultaneous Measurement of Oxygen and Hydrogen Peroxide Fluxes in Permeabilized Cells, Tissue Homogenate and Isolated Mitochondria. Biomolecules. 2015;5(3):1319-38.
4. Frezza C, Cipolat S, Scorrano L. Organelle isolation: functional mitochondria from mouse liver, muscle and cultured filroblasts. Nature Protocols. 2007;2(2):287-95.
5. Kuznetsov AV, Veksler V, Gellerich FN, Saks V, Margreiter R, Kunz WS. Analysis of mitochondrial function in situ in permeabilized muscle fibers, tissues and cells. Nature Protocols. 2008;3(6):965-76.
6. Puka-Sundvall M, Wallin C, Gilland E, Hallin U, Wang XY, Sandberg M, et al. Impairment of mitochondrial respiration after cerebral hypoxia-ischemia in immature rats: relationship to activation of caspase-3 and neuronal injury. Dev Brain Res. 2000;125(1-2):43-50.
7. Savorani F, Tomasi G, Engelsen SB. icoshift: A versatile tool for the rapid alignment of 1D NMR spectra. J Magn Reson. 2010;202(2):190-202.
8. Tomasi G, Savorani F, Engelsen SB. icoshift: An effective tool for the alignment of chromatographic data. J Chromatogr A. 2011;1218(43):7832-40.
9. Dieterle F, Ross A, Schlotterbeck G, Senn H. Probabilistic quotient normalization as robust method to account for dilution of complex biological mixtures. Application in 1H NMR metabonomics. Anal Chem. 2006;78(13):4281-90.
10. Jonsson P, Wuolikainen A, Thysell E, Chorell E, Stattin P, Wikstrom P, et al. Constrained randomization and multivariate effect projections improve information extraction and biomarker pattern discovery in metabolomics studies involving dependent samples. Metabolomics. 2015;11(6):1667-78.
11. Perez MJ, Cederbaum AI. Metallothionein 2A induction by zinc protects HEPG2 cells against CYP2E1-dependent toxicity. Free Radic Biol Med. 2003;34(4):443-55.
12. Guo S, Li ZZ, Gong J, Xiang M, Zhang P, Zhao GN, et al. Oncostatin M Confers Neuroprotection against Ischemic Stroke. Journal of Neuroscience. 2015;35(34):12047-62.
13. Mu D, Chang YS, Vexler ZS, Ferriero DM. Hypoxia-inducible factor 1alpha and erythropoietin upregulation with deferoxamine salvage after neonatal stroke. Exp Neurol. 2005;195(2):407-15.
14. Sheldon RA, Lee CL, Jiang X, Knox RN, Ferriero DM. Hypoxic preconditioning protection is eliminated in HIF-1alpha knockout mice subjected to neonatal hypoxia-ischemia. Pediatr Res. 2014;76(1):46-53.
15. Lushnikova I, Orlovsky M, Dosenko V, Maistrenko A, Skibo G. Brief anoxia preconditioning and HIF prolyl-hydroxylase inhibition enhances neuronal resistance in organotypic hippocampal slices on model of ischemic damage. Brain Res. 2011;1386:175-83.
16. Verma M, Shulga N, Pastorino JG. Sirtuin-4 modulates sensitivity to induction of the mitochondrial permeability transition pore. Biochim Biophys Acta. 2013;1827(1):38-49.

17. Peng Z, Li J, Li Y, Yang X, Feng S, Han S, et al. Downregulation of miR-181b in mouse brain following ischemic stroke induces neuroprotection against ischemic injury through targeting heat shock protein A5 and ubiquitin carboxyl-terminal hydrolase isozyme L1. J Neurosci Res. 2013;91(10):1349-62.
18. Thompson JW, Dave KR, Saul I, Narayanan SV, Perez-Pinzon MA. Epsilon PKC increases brain mitochondrial SIRT1 protein levels via heat shock protein 90 following ischemic preconditioning in rats. PLoS One. 2013;8(9):e75753.
19. Jiao JD, Garg V, Yang B, Hu K. Novel functional role of heat shock protein 90 in ATP-sensitive K+ channel-mediated hypoxic preconditioning. Cardiovasc Res. 2008;77(1):126-33.
20. Yin C, Xi L, Wang X, Eapen M, Kukreja RC. Silencing heat shock factor 1 by small interfering RNA abrogates heat shock-induced cardioprotection against ischemia-reperfusion injury in mice. J Mol Cell Cardiol. 2005;39(4):681-9.
21. Chan JY, Cheng HL, Chou JL, Li FC, Dai KY, Chan SH, et al. Heat shock protein 60 or 70 activates nitric-oxide synthase (NOS) I- and inhibits NOS II-associated signaling and depresses the mitochondrial apoptotic cascade during brain stem death. J Biol Chem. 2007;282(7):4585-600.
22. O'Sullivan JC, Yao XL, Alam H, McCabe JT. Diazoxide, as a postconditioning and delayed preconditioning trigger, increases HSP25 and HSP70 in the central nervous system following combined cerebral stroke and hemorrhagic shock. J Neurotrauma. 2007;24(3):532-46.
23. Jiang T, Yu JT, Zhu XC, Zhang QQ, Tan MS, Cao L, et al. Ischemic preconditioning provides neuroprotection by induction of AMP-activated protein kinase-dependent autophagy in a rat model of ischemic stroke. Mol Neurobiol. 2015;51(1):220-9.
24. Morris-Blanco KC, Cohan CH, Neumann JT, Sick TJ, Perez-Pinzon MA. Protein kinase C epsilon regulates mitochondrial pools of Nampt and NAD following resveratrol and ischemic preconditioning in the rat cortex. J Cereb Blood Flow Metab. 2014;34(6):1024-32.
25. Halestrap AP, Richardson AP. The mitochondrial permeability transition: a current perspective on its identity and role in ischaemia/reperfusion injury. J Mol Cell Cardiol. 2015;78:129-41.
26. Das S, Halushka MK. Extracellular vesicle microRNA transfer in cardiovascular disease. Cardiovasc Pathol. 2015;24(4):199-206.
27. Kefas B, Floyd DH, Comeau L, Frisbee A, Dominguez C, Dipierro CG, et al. A miR-297/hypoxia/DGK-alpha axis regulating glioblastoma survival. Neuro-oncology. 2013;15(12):1652-63.
28. Dharap A, Vemuganti R. Ischemic pre-conditioning alters cerebral microRNAs that are upstream to neuroprotective signaling pathways. J Neurochem. 2010;113(6):1685-91.
29. Brandenburger T, Grievink H, Heinen N, Barthel F, Huhn R, Stachuletz F, et al. Effects of remote ischemic preconditioning and myocardial ischemia on microRNA-1 expression in the rat heart in vivo. Shock. 2014;42(3):234-8.
30. Taylor CJ, Church JE, Williams MD, Gerrand YW, Keramidaris E, Palmer JA, et al. Hypoxic preconditioning of myoblasts implanted in a tissue engineering chamber significantly increases local angiogenesis via upregulation of myoblast VEGF-A expression, and downregulation of miRNA-1, miRNA-206 and Angiopoietin 1. J Tissue Eng Regen Med. 2017.
31. Gao Y, Huang R, Chen R, Li J, Luo W. Ischemic postconditioning altered microRNAs in human valve replacement. J Surg Res. 2016;200(1):28-35.

32. Hu Q, Luo W, Huang L, Huang R, Chen R. Apoptosis-related microRNA changes in the right atrium induced by remote ischemic perconditioning during valve replacement surgery. Sci Rep. 2016;6:18959.
33. Zhao X, Wang K, Hu F, Qian C, Guan H, Feng K, et al. MicroRNA-101 protects cardiac fibroblasts from hypoxia-induced apoptosis via inhibition of the TGF-beta signaling pathway. Int J Biochem Cell Biol. 2015;65:155-64.
34. Varga ZV, Zvara A, Farago N, Kocsis GF, Pipicz M, Gaspar R, et al. MicroRNAs associated with ischemia-reperfusion injury and cardioprotection by ischemic pre- and postconditioning: protectomiRs. Am J Physiol Heart Circ Physiol. 2014;307(2):H216-27.
35. Jiang G, Zhou R, He X, Shi Z, Huang M, Yu J, et al. Expression levels of microRNA-199 and hypoxia-inducible factor-1 alpha in brain tissue of patients with intractable epilepsy. The International journal of neuroscience. 2016;126(4):326-34.
36. Dai BH, Geng L, Wang Y, Sui CJ, Xie F, Shen RX, et al. microRNA-199a-5p protects hepatocytes from bile acid-induced sustained endoplasmic reticulum stress. Cell death & disease. 2013;4:e604.
37. Xu WH, Yao XY, Yu HJ, Huang JW, Cui LY. Downregulation of miR-199a may play a role in 3-nitropropionic acid induced ischemic tolerance in rat brain. Brain Research. 2012;1429:116-23.
38. Chen Q, Xu J, Li L, Li H, Mao S, Zhang F, et al. MicroRNA-23a/b and microRNA-27a/b suppress Apaf-1 protein and alleviate hypoxia-induced neuronal apoptosis. Cell death & disease. 2014;5:e1132.